Transient Liquid Phase Bonding of AlN to AlSiC for Durable Power Electronic Packages

Darshan G. Pahinkar[1*], Waylon Puckett[1], Samuel Graham[1*], Lauren Boteler[2], Dimeji Ibitayo[2], Sreekant Narumanchi[3], Paul Paret[3], Douglas DeVoto[3], Joshua Major[3]

[1]Electronics Manufacturing and Reliability Laboratory, GWW School of Mechanical Engineering, Georgia Institute of Technology, Atlanta, GA 30332

[2]U. S. Army Research Laboratory, Adelphi, MD 20783

[3]National Renewable Energy Laboratory, Golden, CO 80401

[*] Corresponding author – darshan@gatech.edu, sgraham@gatech.edu

771 Ferst Drive NW, Atlanta, GA 30332

ABSTRACT

Conventional power electronic modules employ a direct bonded copper (DBC) substrate and multiple interface layers to dissipate heat. However, reliability issues arise due to the coefficient of thermal expansion (CTE) mismatch that exists between the metal, ceramic, and semiconductor materials in the conventional module. Significant performance enhancement can be achieved by eliminating the DBC and developing an integrated substrate/cold plate with a low CTE mismatch throughout the package. To address this need, we have demonstrated the ability to directly bond the aluminum nitride (AlN) substrate to an AlSiC heat sink through transient liquid phase bonding using a Cu – Al binary system. Fabricated samples are found to have good interfacial adhesion. The novel bond material exhibits properties analogous to AlSiC and is analyzed for thermal, mechanical and metallographic properties. The novel structure demonstrated in this work will enable smaller, lighter, and more reliable power modules, when compared to traditional configurations.

Pursuant to the DOE Public Access Plan, this document represents the authors' peer-reviewed, accepted manuscript. The published version of the article is available from the relevant publisher.

1. INTRODUCTION

Conventional power electronic modules typically employ a direct bond copper (DBC) substrate, three layers of thermal interface materials (TIM), a copper heat spreader, and a heat sink, as shown in Figure 1(a). The DBC consists of an electrical insulator ceramic such as aluminum nitride (AlN) sandwiched on both sides with thick copper (Cu). The presence of multiple layers, contact resistances and low thermal conductivity thermal grease causes two major issues. First, the thermal resistance from device to heat sink remains high, thereby limiting the device power dissipation for a given operating temperature. Secondly, the fatigue performance of the complete package because of multiple layers remains poor due to coefficient of thermal expansion (CTE) mismatch between adjacent layers. For example, Cu in DBC has a CTE of 16×10^{-6} °C^{-1}, whereas the same for AlN is 4.5×10^{-6} °C^{-1}, a ~4X difference. Therefore, as the complete power electronic package is subjected to thermal cycles, an interfacial stress develops at the Cu – AlN boundary. This stress can initially cause deformation, warpage and delamination at the interface and eventually failure of the device. The poor thermal stress performance of DBC in the power electronic package has been widely reported in the literature [1] with DBC having been documented to fail after as few as 100 thermal cycles that range from -40°C to 150°C .

While Cu base plates and Al heat sinks along with direct bonded aluminum (DBA) and DBC are used conventionally, their CTE values remain high as compared to AlN, Si, and SiC. However, mixed matrix composites (MMCs) such as AlSiC have CTE values (as low as 6.5×10^{-6}°C^{-1}) much closer to those of AlN, Si, and SiC ($\approx 4\times10^{-6}$°C^{-1}), thus making them a strong candidate for a power electronic substrate or heat sink without a major loss in thermal performance of the system. Hence, AlSiC heat spreaders can significantly improve reliability, and can be used to replace the Cu and Al heat sink [2]. Furthermore, DBC is typically fabricated using an oxidizing

Pursuant to the DOE Public Access Plan, this document represents the authors' peer-reviewed, accepted manuscript. The published version of the article is available from the relevant publisher.

atmosphere at temperatures above 1070°C [3] and this high processing temperature can result in large residual stresses being induced in the DBC at room temperature, which adds to the driving force for delamination during temperature cycling of the power electronics substrate, leading to lower reliability.

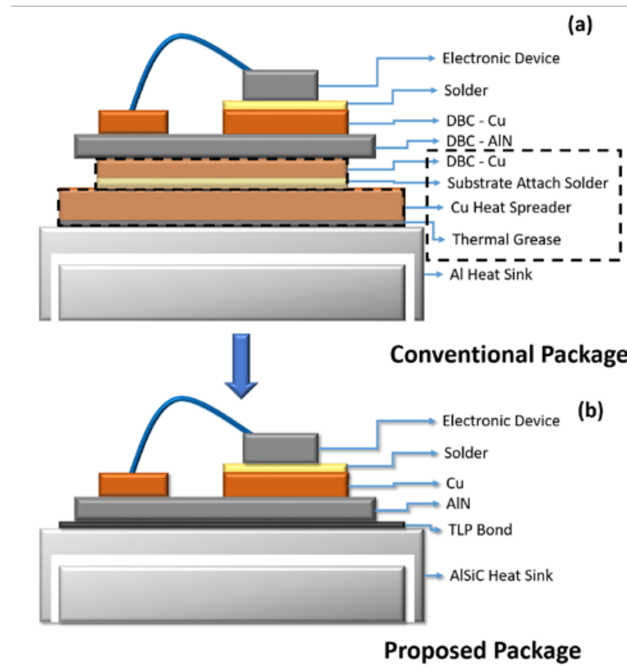

Figure 1. (a) Conventional power electronic package showing device, DBC, base plate and heat sink (b) Proposed package without standard DBC and base plate. Black dotted lines indicate the material layers eliminated as a result of the new stack shown in Figure 1(b).

These concerns can be addressed by eliminating some of the intermediate layers between the electronic devices and the heat sink and replacing Cu with a material that is better matched to AlN in terms of CTE. This modification necessitates exploration of low temperature method for bonding dielectric AlN substrate to composites such as AlSiC in order to create a more durable and low thermal resistance substrate for packaging power electronic devices. By patterning a Cu

Pursuant to the DOE Public Access Plan, this document represents the authors' peer-reviewed, accepted manuscript. The published version of the article is available from the relevant publisher.

circuit layer on top of the AlN and integrating liquid cooling into the AlSiC plate, it is possible to create a new power electronics substrate with a competitive thermal resistance due to the integrated liquid cooling and better fatigue performance due to a low CTE mismatch. Another approach commonly reported in the literature is integrating the cooling mechanisms such as channels or pins into a Cu base plate below the DBC [4] and also in the bottom layer of the DBC without any base plate or heat sink [5]. This approach makes the package more compact, however does not address the CTE mismatch between the DBC layers and the base plate.

To create this bond, we propose to use transient liquid phase (TLP) bonding to create a high thermal conductivity attachment layer at temperatures less than 600°C. The proposed modification in the conventional power electronic package is shown in Figure 1(b). In this work, the new TLP bond is characterized using scanning electron microscopy (SEM) and energy-dispersive X-ray spectroscopy (EDS) to determine the thickness and elemental composition, metallographic properties through the bond layer, respectively. Physical properties such as thermal conductivity, hardness, and elastic modulus of the TLP bond are determined using several experimental methods. Finally, these bond properties are used in computational modeling to assess the advantages of directly bonding the AlSiC heat sink to AlN in a typical IGBT power module.

The key process enabling the bond between the AlN ceramic and the AlSiC cold plate was a transient liquid phase (TLP) bonding process using a Cu – Al eutectic, which is shown in Figure 2. This process entails putting two different metals in contact using a specific bulk ratio, and heating them above the eutectic point, but below the melting temperature of the individual metals [6]. Initially during the heating process, both metals remain solid as they diffuse into each other (Figure 2, state 1). Eventually the composition reaches the liquid regime, allowing a transient liquid state to form (Figure 2, state 2).

Pursuant to the DOE Public Access Plan, this document represents the authors' peer-reviewed, accepted manuscript. The published version of the article is available from the relevant publisher.

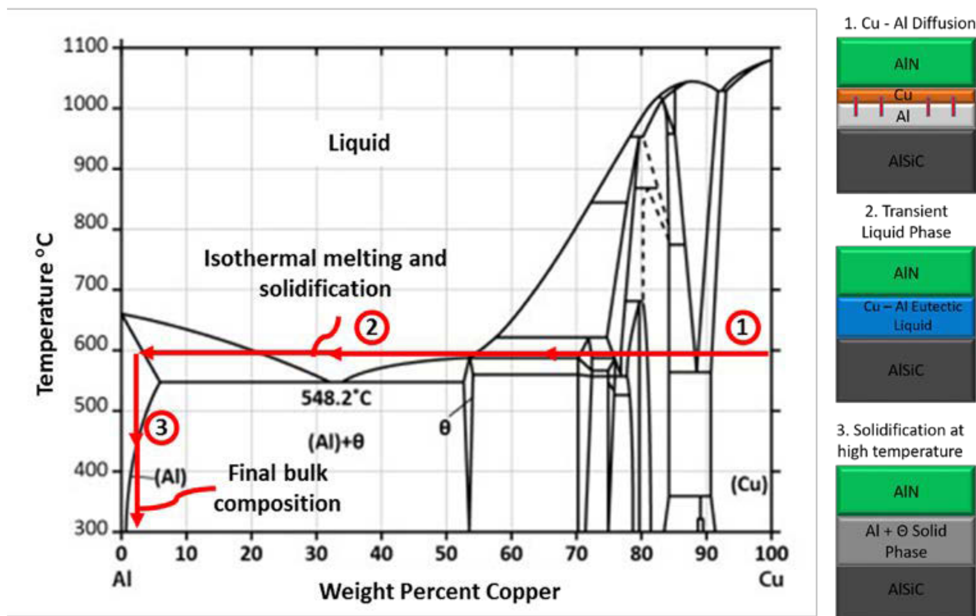

Figure 2. Binary phase diagram and bonding process for copper and aluminum, showing the diffusion and changing composition of the bond layer as Al diffuses into Cu during the heating process. Al and Cu layers are in the ratio of 5:1 by weight, respectively.

As the metals continue to dissolve into the liquid, the composition eventually passes into the liquid/solid regime and partially solidifies. Upon further diffusion, the system eventually begins to solidify completely (Figure 2, state 3). The structure is then left to naturally cool. The final composition is a mixture of Al and θ phase ($CuAl_2$) for a Cu – Al binary system. A similar process was performed by Kuromitsu, Nagatomo, Tonomuru, Akiyama, Montesa, Shibata and Ikuhara [2] to bond bulk Al with AlN and form a direct bonded aluminum (DBA) substrate, in which AlN was coated with Cu by using electron beam deposition for a final bulk composition of 0.2% Cu. However, due to the low Cu content, no θ phase was present in the final bond. The differences between the present method and that by Kuromitsu, Nagatomo, Tonomuru, Akiyama, Montesa, Shibata and Ikuhara [2] is the preparation of the bonding stack, bonding temperatures and finally the base plate itself, i.e., AlSiC. The interaction of AlSiC with the bonding interlayer and AlN is

Pursuant to the DOE Public Access Plan, this document represents the authors' peer-reviewed, accepted manuscript. The published version of the article is available from the relevant publisher.

one of the unique features of the present work, which will be discussed in details in following sections.

2. SAMPLE FABRICATION

The bonds were made by using Al and Cu foils in 5:1 ratio between an AlN ceramic and an AlSiC base plate, as shown in Figure 3. The use of foils made the process fairly simple and inexpensive. The AlSiC layer also had a cover layer of Al 356 alloy (between 50 to 80 μm thick) on the bulk AlSiC, which had 6.5 – 7.5% Si by weight. The initial composition of the bond based on the Al and Cu layer and the Al 356 layer was 77.9% Al, 20.2% Cu, and 1.9% Si by weight. The stack sequence was chosen such that the surface contacting the AlN would initially be pure Cu, and the composition would change according to the arrow shown in Figure 2. This forced the layer directly next to the AlN to pass fully through the liquid regime minimizing possibilities of unbonded areas.

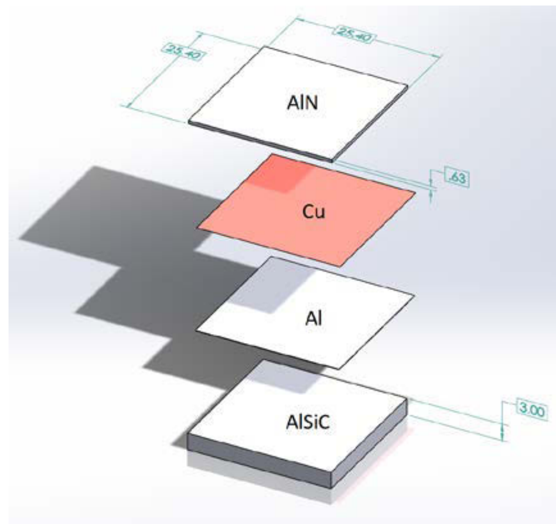

Figure 3. Bonding stack showing the sequence and size of the AlN, Cu, Al, and AlSiC layers. Dimensions are in mm.

Pursuant to the DOE Public Access Plan, this document represents the authors' peer-reviewed, accepted manuscript. The published version of the article is available from the relevant publisher.

In order to ensure that there were no contaminants within the bond, all the participating layers shown in Figure 3 were first cleaned with a 25% hydrochloric acid (HCl) solution at room temperature, followed by being rinsed with deionized (DI) water, and isopropanol or acetone. The HCl solution helped in minimizing aluminum oxide, which may have formed on the Al and AlN, while not affecting the bulk AlN [7]. After cleaning each layer, the stack was placed in a graphite rig. The rig was tightened to hold the samples in place using a clamping force of 2 kN to keep the layers flat and assist with diffusion of components at high temperature. Application of clamping force was deemed necessary as the adhesion without applying the clamping force was found to be weak and the interfaces separated during metallographic preparation for SEM analysis. The rig was then placed in a tube furnace, which was sealed and held under vacuum to a pressure of approximately 20 µTorr (0.0026 Pa). Vacuum was used to minimize the formation of oxides within the bond layer, when the temperatures within the structure were high. The temperature was increased to 530°C in 40 minutes and was held for 30 minutes. In the next step, it was increased to 565°C within 15 minutes and was held for 40 more minutes. Afterwards, the power was turned off allowing the rig to cool naturally to ambient. The hold time at 530°C (30 minutes) was used to allow the Cu to diffuse into the Al before reaching the melt temperature. In this way, when the melt temperature was finally reached, the bond would melt more homogenously as opposed to melting at a small interface layer first, and the liquid layer slowly growing. The hold time of 30 minutes for this step was determined by using Eqs. (1) and (2) using a finite difference calculation explained as follows.

The solid-state diffusion of Cu is governed by Fick's second law given by Eq. (1).

$$\frac{dC}{dt} = D\frac{d^2C}{dx^2} \qquad (1)$$

Pursuant to the DOE Public Access Plan, this document represents the authors' peer-reviewed, accepted manuscript. The published version of the article is available from the relevant publisher.

In this equation, C is the concentration, D is the diffusion coefficient, t is time, and x is the spatial dimension, which is the thickness of the layers in a 1-D format. The diffusion coefficient is dependent on the two diffusing materials, and is a function of time given by Eq. (2):

$$C_d = C_o e^{\frac{-Q_d}{RT}} \tag{2}$$

where C_o is a material constant, (6.5×10^{-5} m^2 s^{-1} for the Al-Cu system), Q_d is the activation energy for diffusion, (136 kJ mol^{-1} for the Al-Cu system), R is the universal gas constant, and T is the temperature [8]. As C_d exponentially increases with T, it is clear that at high temperatures diffusion speed increases rapidly. By modeling the Al-Cu system with these equations, an estimate for the required diffusion time before melting occurred was determined. For the models a time step of 0.001 s, and a spatial step size of 0.1 μm were applied, with the diffusion coefficient recomputed for each temperature. The process temperature was decided to be 530°C to avoid possible overshoot into the liquid regime before diffusion was complete, while also being high enough to allow for rapid diffusion. While this process temperature may seem high, it is substantially lower than the 1074°C processing temperature used to bond DBC. Applying this temperature profile to the numerical model resulted in a final composition profile through the Cu and Al layer as shown in Figure 4.

Pursuant to the DOE Public Access Plan, this document represents the authors' peer-reviewed, accepted manuscript. The published version of the article is available from the relevant publisher.

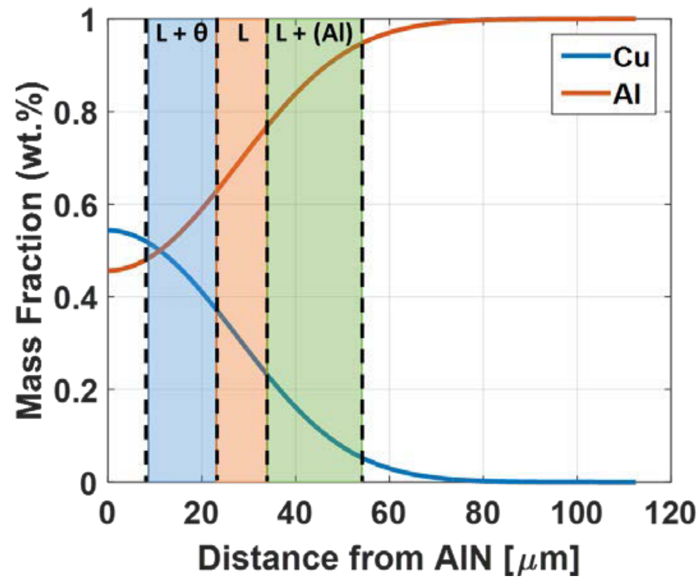

Figure 4. Composition of the Al-Cu layers as a function of distance from the AlN layer at the time when the temperature reaches 565°C (85 minutes). This shows the regime, which is purely liquid, the liquid + θ regime, and the liquid + Al regime.

According to this result, at the time when the temperature reached 565°C, approximately 35 μm of the bond thickness turned to mostly liquid. This pre-diffusion step provides advantages over simply increasing to the melt temperature immediately. First, by decreasing the amount of liquid, which formed at one time, the effect of leakage was reduced. Here, leakage means liquid metal attempting to escape the graphite rig, due to applied pressure on the layers and vacuum in the furnace. The early liquid composition had a high Cu content, so if a thin liquid interface layer leaked, it would take a disproportionately large amount of Cu with it.

The sample was removed from the furnace, when it reached ambient temperature. In order to prepare the sample for SEM imaging, its edges were polished and cleaned with sonication for 30 minutes. A photograph of a bonded sample is shown in Figure 5, which shows the polished edge.

Pursuant to the DOE Public Access Plan, this document represents the authors' peer-reviewed, accepted manuscript. The published version of the article is available from the relevant publisher.

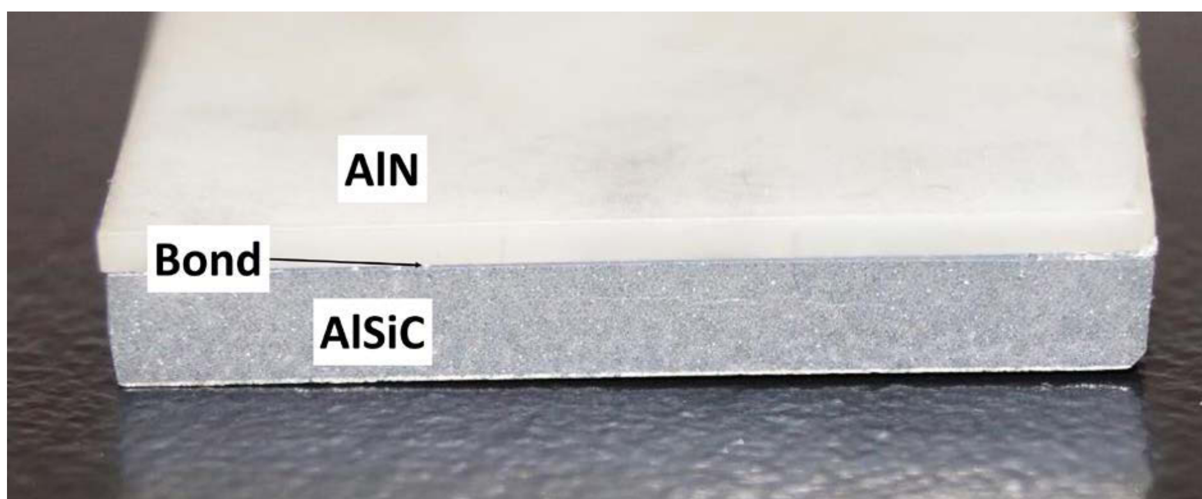

Figure 5. Photograph of the polished transverse section of the bond showing AlN, bond and AlSiC layers (From top).

3. SEM AND EDS ANALYSIS

Scanning electron microscopy (SEM) was used to image the bond between the AlN and the AlSiC, while energy-dispersive X-ray spectroscopy (EDS) was used to determine the bond composition quantitatively. As shown in Figure 6, an unexpected result revealed that some of the SiC particles migrated into the bond showing that the TLP bond reacted with the AlSiC plate and the liquid layer allowed SiC to freely move. This resulted in the formation of a metal matrix composite bond, which is different from other TLP methods shown for joining AlN and Al. By evaluating SEM images at several locations across the bond, it was found that the average bond thickness was 140 μm, which is greater than the initial starting Al-Cu layers used to initiate the bond (~100 μm thick). Using the EDS image the composition of the bond area was found to be 93.0% Al, 0.6% C, 1.5% Cu, 0.3% N, 1.7% O, and 2.8% Si by weight.

Pursuant to the DOE Public Access Plan, this document represents the authors' peer-reviewed, accepted manuscript. The published version of the article is available from the relevant publisher.

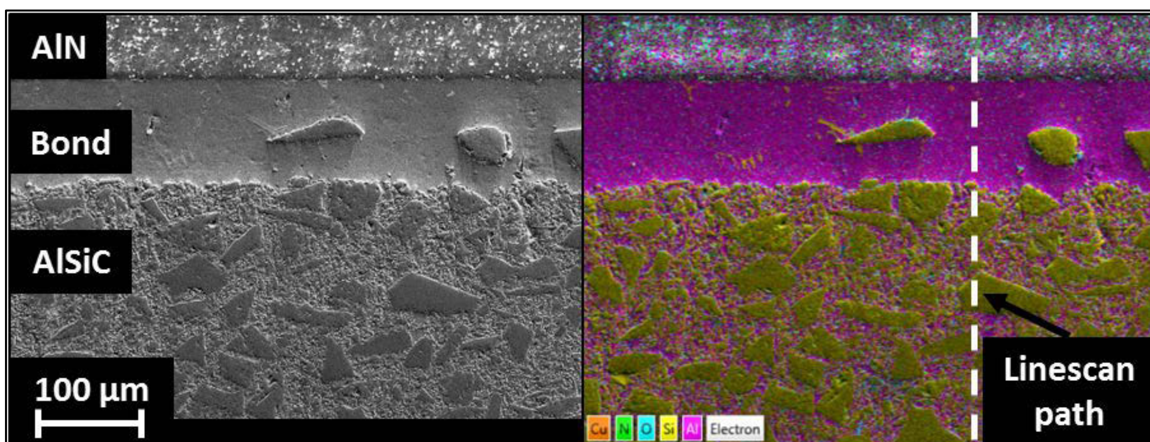

Figure 6. SEM (Left), and EDS (Right) images showing the AlN on top with the bond, and SiC particles, some of which have drifted into the bond line. The EDS image also indicates the path followed for the linescan analysis with a dotted line.

Using the binary phase diagram in Figure 2 with 1.5% Cu, the ratio of the θ phase or $CuAl_2$ was estimated to be 2.8%, with Al + Cu + Si being 97.2% by weight. This differs significantly from the estimation based only on the materials in the intermediate layers only (77.9% Al, 20.2% Cu, and 1.9% Si by weight). This difference is due to the exclusion of the Al in Al-356 of the AlSiC matrix, which accounts for 37% of the bulk 3 mm thick AlSiC, the rest being SiC. It must be noted that the initial composition and associated calculations were made to analyze the diffusion of Cu in Al just to ensure that before completely melting the Cu – Al bulk interlayer, sufficient cross diffusion of elements has occurred. The revised estimate of composition is a result of solid-state diffusion as well as liquid interlayer interacting with the AlSiC. Including this amount of Al in AlSiC, the estimation becomes 92.9% Al, 1.3% Cu, and 5.8% Si by weight. This composition is now similar to the mass fractions measured with EDS, implying that melting occurred deeply within the AlSiC matrix. Through EDS imaging of the backside of the AlSiC, trace amount of Cu was confirmed, which corroborated the important inference that Al in the AlSiC matrix takes part

Pursuant to the DOE Public Access Plan, this document represents the authors' peer-reviewed, accepted manuscript. The published version of the article is available from the relevant publisher.

in bonding and Cu diffused deep into AlSiC matrix. While the migration of SiC particles in the bond material are suggestive of the same conclusion, their presence in the bond is expected to avoid the bond flowing plastically at elevated temperatures and locally enhance the thermal conductivity, as k_{SiC} is of the same order as that of pure Cu.

In order to track the diffusion of different species through the depth of the bond, an EDS linescan was used as shown in Figure 7(a). This measurement was performed at several different locations, but only one representative location is shown, as all scans had similar results. The SiC particles are indicated in Figure 7(a) by the spikes in Si within the AlSiC layer, which was known because of the simultaneous spikes in carbon. However, this particular Si spike in the bond region was not accompanied by a spike in carbon. It means that it was from the Al 356 alloy. Another interesting and unexpected observation was the diffusion of Al metal into an AlN crystal structure as the 1:1 molar ratio (Al:N) should have remained constant. Therefore this was investigated further by analysis of pure AlN not used in bonding and the results are compared in Figure 7(b).

The Al concentration within the pure AlN sample can be seen in Figure 7(b) to be constant through the AlN with almost zero slope of the Al concentration. However, the bonded AlN sample clearly shows an increase in the Al concentration closer to the AlN-Bond interface with a 25 times larger slope than the un-bonded sample. This confirmed that the Al was found into the AlN substrate. This migration was thought to have occurred because AlN substrates are manufactured by sintering AlN particles together using a yttria (Y_2O_3) additive to reduce the processing temperature and aid in densification [9]. Therefore, there were grain boundaries and voids within the AlN, which the molten bond material was able to fill. Although this is advantageous for the bond strength by improving adhesion, Al metal diffusing deep into the AlN can potentially affect

Pursuant to the DOE Public Access Plan, this document represents the authors' peer-reviewed, accepted manuscript. The published version of the article is available from the relevant publisher.

the dielectric properties of AlN. Therefore, it was necessary to evaluate the dielectric strength of AlN to ensure that the bonding process does not compromise it.

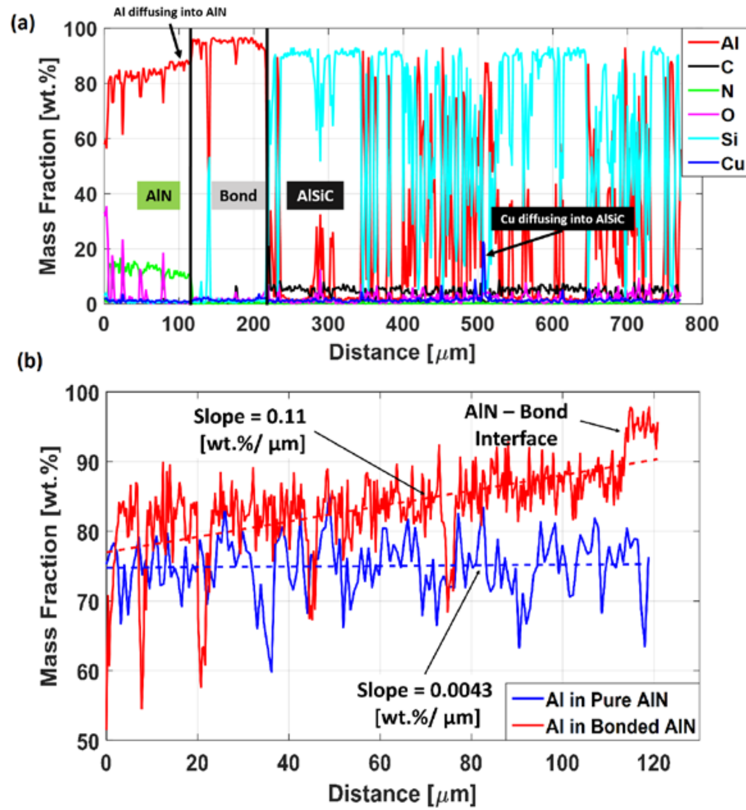

Figure 7. (a) EDS linescan results showing the three distinct regions of AlN, the bond, and the AlSiC. This plot also shows the diffusion of Cu as far as 300 μm into the AlSiC, and the diffusion of Al into the AlN as indicated in the plot (b) Plot of mass fraction of Al through the AlN substrate for both an un-bonded and bonded AlN showing the slope of the line computed with linear regression.

4. DIELECTRIC STRENGTH

In order to test the dielectric strength, two copper electrodes were attached to either side of the bonded sample with copper tape. A voltage was then applied and increased, until current began to flow through the AlN. Because the dielectric breakdown strength of air was much less than the AlN, the sample needed to be submerged in a dielectric fluid. Therefore, Fluorinert (FC-72) from

Pursuant to the DOE Public Access Plan, this document represents the authors' peer-reviewed, accepted manuscript. The published version of the article is available from the relevant publisher.

3M, a dielectric fluid with a strength of 15 kV mm^{-1} was used. As the electrodes were placed at about 5 mm from the edges of the sample, the FC-72 had a total blocking voltage of approximately 150 kV. While submerged, the AlN began to conduct electricity at 18 kV, leading to a dielectric strength of 17.7 kV mm^{-1} for an AlN substrate with a thickness of 1.02 mm. The test was then repeated with an un-bonded sample of AlN, and as expected, dielectric breakdown occurred at 18 kV. This value was also consistent with the AlN manufacturer specified value of 17 kV mm^{-1} for the dielectric strength [10]. These tests conducted on multiple samples confirmed that neither the bonding process nor the leakage of Al into the AlN grains reduces the dielectric strength of the AlN after bonding and occurrence of Al in AlN was predominately a function of surface roughness of AlN.

5. YOUNG'S MODULUS AND HARDNESS

It is important to understand the mechanical behaviour of the bond material, so that it can be modelled for thermally induced stresses. Therefore, the hardness (H) and the Young's modulus (E) were both measured with a diamond tipped nanoindenter (Hysitron Ti 900 Triboindenter) that was calibrated with fused silica. The calibration was performed over a range of 0 to 600 nm indentation distance, encompassing the full range of 0 to 500 nm, which was displaced by the bond material. In order to test the properties of the bond material alone, a new sample was made with the AlSiC substrate coated with Al and Cu, but without the AlN layer. Thus, the equivalent material composition was produced, but there was a larger area to access the bond material. After sample fabrication, the topside of the bond material was polished with the same procedure used to prepare the sample for SEM imaging. To extract E and H of the bond material, nine indentations per run in a 90 by 90 μm grid array were made. For each indentation, a loading/unloading curve was generated, and values of E and H were extracted and plotted in Figure 8(a) and (b), respectively.

Pursuant to the DOE Public Access Plan, this document represents the authors' peer-reviewed, accepted manuscript. The published version of the article is available from the relevant publisher.

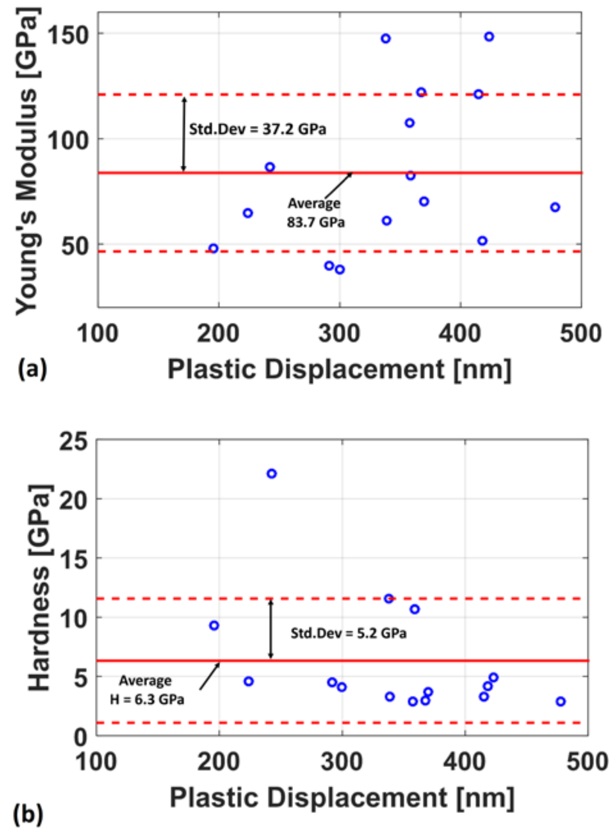

Figure 8. (a) Plot of Young's Modulus showing the average of 83.7 GPa with a solid red line, and the standard deviation of 37.2 GPa with dotted red lines. (b) Plot of Hardness showing the average of 6.3 GPa with a solid red line, and the standard deviation of 5.2 GPa with dotted red lines.

When compared to pure Al, which has an E value of 75 GPa, the bond material is slightly more rigid. This is possibly due to the bond being a mixture of Al and the θ phase, ($CuAl_2$), which has modulus of 120 GPa [11]. Another cause could have been the SiC particles near the surface, which have a modulus of 410 GPa, and could have aided in resistance to elastic deformation. The large standard deviation in the data was also attributed to the SiC particles, which on the length scale of 90 µm of the area chosen for observation, are not uniformly distributed beneath the surface. Each SiC particle could be as large as 80 µm or as small as 1 µm.

Pursuant to the DOE Public Access Plan, this document represents the authors' peer-reviewed, accepted manuscript. The published version of the article is available from the relevant publisher.

The hardness of the bond was measured to be 6.3 GPa, and was significantly larger than the hardness of Al of 0.5 GPa. However, the value was also much smaller than the hardness of SiC, being 28 GPa and greater than the typical values of the hardness for Sn-Ag-Cu solders of 2 GPa [12]. The increase in hardness was due to precipitate hardening, which introduced precipitates, (the 2.8 % θ phase), into the matrix to obstruct the movement of dislocations [13]. Since the hardness is a measure of the materials resistance to permanent plastic deformation, this increase implies this bond would be much more resistant to permanent deformation than a pure Al bond or even conventional solders. The hardness also had a large standard deviation, which again could be due to the SiC particles spread non-uniformly beneath the surface.

6. THERMAL CONDUCTIVITY

Another important thermo-physical property of the bond is the thermal conductivity as this parameter dominates the thermal transport abilities of the material. It was measured with a laser flash diffusivity technique. Laser flash diffusivity is a transient heat flow measurement, wherein one side of a sample absorbs a short laser pulse, while the temperature change on the other side is monitored. This temperature change as a function of time can then be fitted to analytical models to compute the thermal diffusivity of the material.

In order to determine the thermal diffusivity and in turn the thermal conductivity of the bond material, the thermal diffusivity of both the AlN and AlSiC were first measured with the laser flash diffusivity method using the Hyperflash system. All samples were coated with a thin graphite layer (up to 10 μm) to increase the emissivity of the surface. The sample holder was made of insulating ABS plastic to reduce the heat loss at the edges. The experiment was conducted in a vacuum-sealed chamber held at 25°C to eliminate variation from ambient temperature changes. For the single layer materials, thermal diffusivity was computed with a model by Cowan [14]. The bonded

Pursuant to the DOE Public Access Plan, this document represents the authors' peer-reviewed, accepted manuscript. The published version of the article is available from the relevant publisher.

samples were then measured the same way, and using the measured thermal diffusivity for pure AlN, and pure AlSiC; the thermal diffusivity of the bond layer was determined. The flash was repeated three times and an average thermal diffusivity is reported. The material thermal diffusivity, density, heat capacity, and thermal conductivity are reported in Table 1. The density of the bond was computed as the weighted average between the density of Al, 2700 kg/m^3, and the density of $CuAl_2$, 4400 kg/m^3, using the estimated ratio of 97.2% Al, and 2.8% $CuAl_2$, estimated from the EDS analysis earlier [15]. The effective thermal conductivity value of the bondline was found to be 121.2 ±5.3 W m^{-1} K^{-1}, which is about two times better than typical solders and about a 100 times better than standard TIM materials.

Table 1. Thermo-physical properties of the substrate materials.

Material	Thermal Diffusivity (m^2 s^{-1})	Density (kg m^{-3})	Specific Heat (J kg^{-1} K^{-1})	Effective Thermal Conductivity (W m^{-1} K^{-1})
AlSiC	$7.94\times10^{-5} \pm 2.1\times10^{-7}$	2870	741	168.8 ± 0.5
AlN	$6.47\times10^{-5} \pm 2.0 \times10^{-5}$	3260	740	156.1 ± 0.5
Bond	**$5.17\times10^{-5} \pm 2.3\times10^{-5}$**	**2750**	853	**121.2 ± 5.3**

The thermal conductivity of the bond material was also measured using a Time-Domain Thermoreflectance (TDTR) approach. The sample used for nanoindentation tests was used for TDTR measurements and was coated with Al layer of 80 nm thick after fine polishing. The thermal conductivity of the bond material was found to be 133 ± 12 W m^{-1} K^{-1} and was slightly higher than the effective thermal conductivity of the bondline (121.2 W m^{-1} K^{-1}). This is possible because, the Laser Flash diffusivity measurement also included the contact resistance of the bond and effect of

Pursuant to the DOE Public Access Plan, this document represents the authors' peer-reviewed, accepted manuscript. The published version of the article is available from the relevant publisher.

voids. Nevertheless, it should be noted that the effective thermal conductivity and the material thermal conductivity of this bond layer was higher than that of most solders (≈ 50 W m^{-1} K^{-1}) and thus is expected to provide a lower thermal resistance than if materials such as AuSn were used to join the AlN and AlSiC.

7. THERMAL PERFORMANCE

Once the thermal conductivity of the bond material was determined, thermal modeling and heat spreading analysis was conducted to assess the performance of the new TLP bond in comparison with the DBC-based stacking. A section of Toyota Prius inverter geometry [16] was selected for this study, as shown in Figure 9(a). The complete package dissipates 2400 W of heat using 12 pairs of an IGBT and a diode. Due to symmetry conditions and to save computational cost, heat transfer in two pairs in an identical section of the total package as shown in Figure 9(b) was simulated. Additionally, instead of applying the convection boundary condition at the backside of the base plate, fluid modeling was incorporated in the simulations. The coolant used for simulations was water – ethylene glycol (50/50) [17].

The details of the fluid modeling and selection of the cooling methodology and optimum geometry features are discussed in detail by Pahinkar *et al.* [18] , wherein minichannel geometry was determined to provide better heat transfer coefficient than pin fins and spray cooling for a fixed given coolant pumping power. The summary of the fluid flow modeling and boundary conditions adapted in the present work are shown in Table 2. These conditions are applied exactly to different stacking configurations shown in Figure 10 for comparison of thermal performance between the TLP bond – AlSiC configuration and DBC-AlSiC configuration.

Pursuant to the DOE Public Access Plan, this document represents the authors' peer-reviewed, accepted manuscript. The published version of the article is available from the relevant publisher.

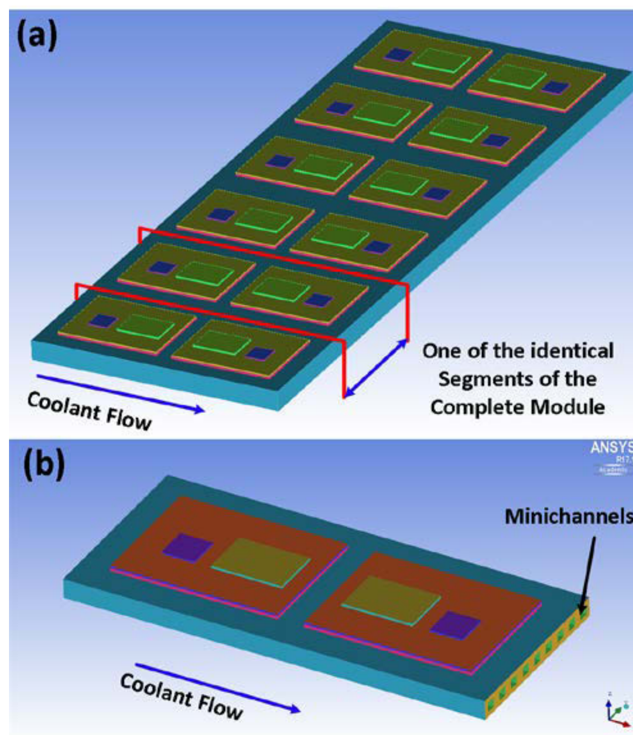

Figure 9. (a) Toyota Prius inverter package (b) An identical section of the package selected for Computational Fluid Dynamics (CFD) and Heat Transfer (HT) simulation showing minichannels drawn in the AlSiC base plate.

Pursuant to the DOE Public Access Plan, this document represents the authors' peer-reviewed, accepted manuscript. The published version of the article is available from the relevant publisher.

Table 2. Fluid boundary conditions and channel geometry details selected for modeling the heat spreading and removal.

Parameter	Value
Total heat dissipated	400 W
IGBT heat flux	120 W cm^{-2}
Diode heat flux	95 W cm^{-2}
Coolant	Water - ethylene glycol
Coolant density	999 kg m^{-3}
Coolant specific heat	3820 J kg^{-1} K^{-1}
Coolant conductivity	0.391 W m^{-1} K^{-1}
Coolant viscosity	0.0011 N s^{-1} m^{-1}
Coolant Pumping power	8 W
Coolant mass flow rate	0.2 kg s^{-1}
Square minichannel side	2 mm
Coolant inlet temperature	80°C
Si thickness, IGBT	510 µm
Si thickness, Diode	320 µm
Solder thickness	100 µm
Cu layer thickness	300 µm
AlN thickness	630 µm
Bond thickness	140 µm
AlSiC thickness	3 mm

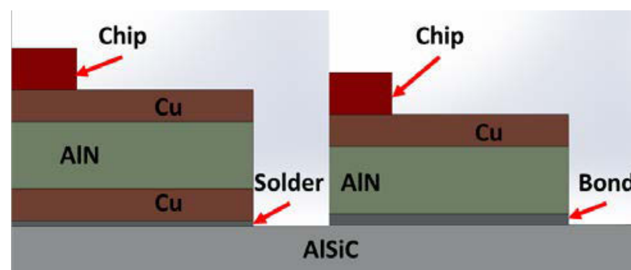

Figure 10. A power package stack showing the location of the DBC, and solder (Left), compared to replacing the Cu and solder layers with the TLP bond (Right).

Pursuant to the DOE Public Access Plan, this document represents the authors' peer-reviewed, accepted manuscript. The published version of the article is available from the relevant publisher.

The computational model was developed and meshed in ANSYS ICEMCFD and simulated in ANSYS FLUENT^{TM}. Grid independence was ensured and the conservation equations were solved until they converged within 0.5%. Figure 11 shows the temperature contours of the power electronic package with DBC and with the TLP bond.

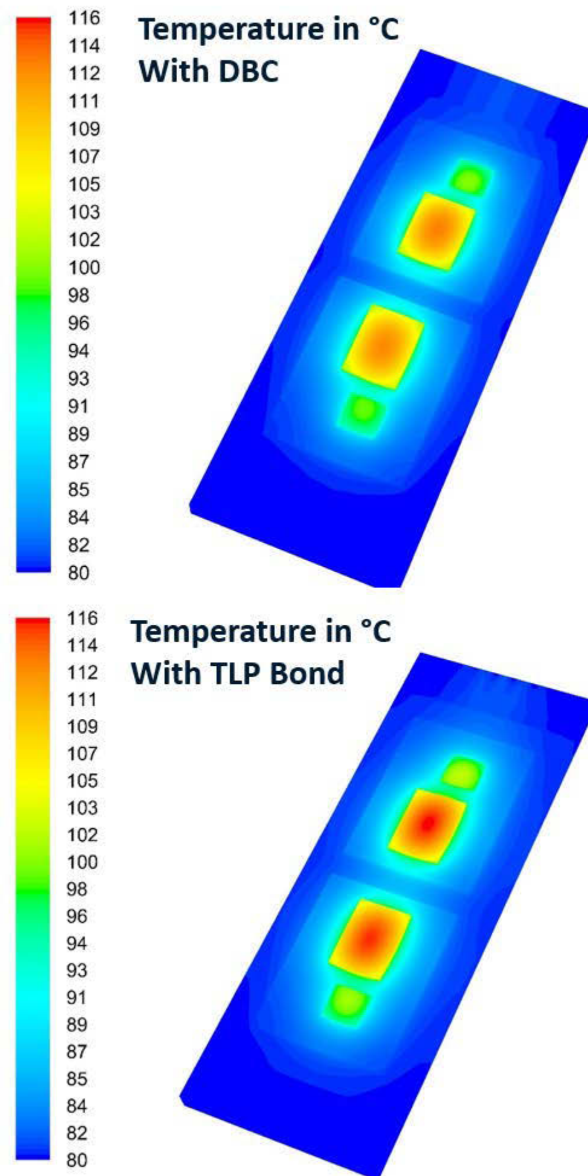

Figure 11. Temperature contours with DBC (top) and with TLP bond (bottom) showing a maximum device temperature rise of 33°C and 36°C, respectively.

Pursuant to the DOE Public Access Plan, this document represents the authors' peer-reviewed, accepted manuscript. The published version of the article is available from the relevant publisher.

The device temperature was greater for the TLP bond-based system than the DBC-based stack by 3°C, as ΔT_{Max} for the DBC stack was 33°C, while that with the TLP bond was 36°C. This increase was because of removal of the Cu layer at the bottom of the AlN in the DBC, which aided in heat spreading directly below AlN. The bond material thermal conductivity of 121.2 W m^{-1} K^{-1} indicates its standalone thermal performance, however the device temperature depends heavily on how fast and efficiently heat is spread after it leaves the device. The bottom Cu layer in the DBC helps in spreading heat more effectively after it leaves AlN in the lateral direction. This is not the case with the thin AlSiC bond (100 µm) with a thermal conductivity of 121.2 W m^{-1} K^{-1}, replacing the thick Cu layer (300 µm) and a thermal conductivity of 401 W/m-K. While the linear thermal resistance between the device and the heat sink with this bond decreases as compared to that with DBC, yet heat spreading is marginally affected due to removal of the DBC Cu layer.

Simultaneous modifications in the heat flux input and cooling methods yielded the exact temperature difference between devices for these two configurations, hence a comparative parametric study was not required. Despite the fact that DBC-based stack yielded marginally better device temperature for the same pumping power, the TLP bond stack is expected to provide a better fatigue and reliability performance. This is because as a Cu layer with a CTE of 16 ppm $°C^{-1}$ is removed and is replaced by a TLP bond that has more favorable mechanical properties described in the preceding section.

8. FATIGUE AND THERMAL STRESS

Multiple samples were tested for observation of thermal stresses at interfaces. Multiple samples were tested for fatigue tests cycling between -40°C and 150°C with a heating and cooling rate of 5°C/min and aging tests were conducted at 150°C. These test parameters are based on JEDEC Standard Temperature Cycling - Standard JESD22-A104D, which is a widely accepted set

Pursuant to the DOE Public Access Plan, this document represents the authors' peer-reviewed, accepted manuscript. The published version of the article is available from the relevant publisher.

of fatigue cycle parameters to evaluate the reliability of the substrate – baseplate attach materials. All samples showed no change in void fraction even after 1400 fatigue cycles and 1400 hours of aging tests, without any question of delamination. Comparing this performance with that of the DBC failing at as early as 100 cycles, it can be safely concluded that the AlN-AlSiC configuration yields much superior mechanical performance than the DBC-based power packages.

9. CONCLUSION AND FUTURE WORK

A method for bringing the cooling solution closer to the device was investigated that involved bonding the AlN dielectric layer directly to an AlSiC base plate. Using SEM imaging and EDS analysis the bond was shown to be composed of 93.0% Al, 0.6% C, 1.5% Cu, 0.3% N, 1.7% O, and 2.8% Si by weight, meaning the Cu had diffused through the bulk of the AlSiC layer. The aluminum was also seen to migrate into the AlN layer approximately up to 100 μm, leading to a strong bond between the AlN and the AlSiC. The dielectric blocking strength of the AlN/AlSiC was then measured to be the same as the as received AlN, so the processing did not affect the dielectric properties of the AlN. The Young's modulus was measured to be 83.7 GPa, with a hardness of 6.3 GPa, which were both higher than pure Al and solders, making the bonds more resistant to deformation. The effective thermal conductivity of the bond was found to be 121.2 W m^{-1} K^{-1} using Laser Flash approach. This is approximately twice that of solder, with an average thickness of 100 μm. The device temperature with the TLP-bond was found to be greater than 3°C than that with the DBC, when the pumping power, mass flow rate and other simulation parameters were kept constant. However, with a minor increase in mass flow rate, this minor difference could be eliminated, considering that this TLP bond yields high heat dissipated per unit volume, per unit weight and per unit cost with enhanced fatigue performance. Finally, samples were thermally cycled and were found to manifest no significant change even after 1400 cycles between -40°C,

Pursuant to the DOE Public Access Plan, this document represents the authors' peer-reviewed, accepted manuscript. The published version of the article is available from the relevant publisher.

and 150°C, which was approximately more than 14 times the typical lifetime of DBC for the same cycling range. Aging tests on multiple samples showed no change in void fraction after 1400 cycles. Therefore, this bonding method maintains almost similar thermal performance to DBC, while improving the lifetime, and reducing stresses in the device by a great margin.

The ongoing and future work involves investigation of bonding parameters, such as surface roughness of the AlN, Cu/Al relative mass fractions in the bond interlayer on the resultant bond strength, bond void fraction and effective thermal conductivity. Refinement in terms of void fraction can further enhance the benefits of this bonding technique. After the bond material characterization in terms of fatigue, shear and aging tests is complete, commercial fabrication of complete packages based on this technique can follow. Minichannels or pin fins can be carved into the AlSiC heat sink, followed by directly bonding this AlSiC heat sink/base plate to the AlN using the TLP bonding method outlined in the present work. Cu layer on top of AlN can be included using either additive manufacturing techniques or metal deposition. While methods to attach the electronic device to Cu-circuit layer can include the convectional die-attach materials, further exploration of the present technique in terms of lower temperature TLP bonds, such as CuSn can result in elimination of die-attach solders as well. This work is also currently under investigation by the authors.

Another aspect in the validation of this work is the comprehensive comparison of the device temperatures with the modified power electronic package and those with the conventional packages as shown in Figure 11. This approach coupled with the fatigue and aging tests can provide a quantitative basis to assert the comprehensive benefits of this TLP bonding approach.

Pursuant to the DOE Public Access Plan, this document represents the authors' peer-reviewed, accepted manuscript. The published version of the article is available from the relevant publisher.

10. ACKNOWLEDGEMENTS

The authors would like to thank the U.S. Army Research Laboratory and the National Renewable Energy Laboratory for sponsoring this work. The contribution of Zhe Cheng and Dr. Thomas Bougher from Heat lab, Georgia Tech for the thermal conductivity measurement is gratefully acknowledged.

11. KEYWORDS

Power electronics, thermal management, transient liquid phase bonding, characterization.

12. REFERENCES

[1] a) D. DeVoto, M. Mihalic, T. Popp, S. Narumanchi, presented at IEEE Int. Accel. Stress Test. Reliab. Workshop, San Francisco, CA **2011**; b) L. Dupont, *M.S. Thesis* École normale supérieure de Cachan - ENS Cachan, 2006-06-22, **2006**; c) S. Pietranico, S. Pommier, S. Lefebvre, S. Pattofatto, *Int. J. Fatigue* **2009**, 31, 1911.

[2] Y. Kuromitsu, Y. Nagatomo, H. Tonomuru, K. Akiyama, C. M. Montesa, N. Shibata, Y. Ikuhara, in *Int. Conf. Integr. Power Electron. Syst.*, VDE VERLAG GMBH, Nuremberg/Germany 2010.

[3] M. Entezarian, R. A. L. Drew, *Mater. Sci. Eng.* **1996**, 212, 206.

[4] a) Y. Wang, S. Jones, A. Dai, G. Liu, *Microelectron. Reliab.* **2014**, 54, 1911; b) A. Bar-Cohen, J. J. Maurer, J. G. Felbinger, in *Int. Conf. Compd. Semicond. Manuf. Technol.*, New Orleans, Louisiana, USA 2013.

[5] A. Sakanova, S. Yin, presented at IEEE Electron. Packag. Technol. Conf., 15th, 11-13 Dec. 2013, **2013**.

[6] W. MacDonald, T. Eagar, *Annu. Rev. Mater. Sci.* **1992**, 22, 23.

[7] C. Deitch, A. Crawford, A. Meier, R. Fagan, *Mater. Manuf. Processes* **2005**, 20, 863.

[8] W. F. Gale, T. C. Totemeier, *Smithells metals reference book*, Butterworth-Heinemann, **2003**.

[9] M. Medraj, Y. Baik, W. T. Thompson, R. A. L. Drew, *J. Mater. Process. Technol.* **2005**, 161, 415.

[10] Aluminum NItride Engineering Properties, http://accuratus.com/alumni.html, accessed: 2017.

Pursuant to the DOE Public Access Plan, this document represents the authors' peer-reviewed, accepted manuscript. The published version of the article is available from the relevant publisher.

[11] J. Zhang, Y. N. Huang, C. Mao, P. Peng, *Solid State Commun.* **2012**, 152, 2100.

[12] T. Siewert, S. Liu, D. R. Smith, J. C. Madeni, in *Properties of Lead-Free Solders Release 4.0* (Ed: N. I. o. S. a. T. C. S. o. Mines), Colorado 2002.

[13] J. P. Schaffer, A. Saxena, S. D. Antolovich, T. H. Sanders, S. B. Warner, *The science and design of engineering materials*, Irwin Chicago, **1995**.

[14] R. D. Cowan, *J. Appl. Phys.* **1963**, 34, 926.

[15] S. Aksöz, Y. Ocak, N. Maraşlı, E. Çadirli, H. Kaya, U. Böyük, *Exp. Therm. Fluid Sci.* **2010**, 34, 1507.

[16] N. Malu, D. Bora, S. Nakanekar, S. Tonapi, presented at ITherm 2014 Proc., Intersoc. Conf. Therm. Thermomech. Phenom. Electron. Syst., 14th, 27-30 May 2014, **2014**.

[17] CERN, Properties of mixture Water/Glycol, http://detector-cooling.web.cern.ch/Detector-Cooling/data/Table%208-3-1.htm, accessed: 11/25/2017.

[18] D. G. Pahinkar, W. Puckett, S. Graham, L. Boteler, D. Ibitayo, presented at IEEE WiPDA 2017 Wide Bandgap Power Devices and Appl., Oct. 30 2017-Nov. 1 2017, **2017**.

Pursuant to the DOE Public Access Plan, this document represents the authors' peer-reviewed, accepted manuscript. The published version of the article is available from the relevant publisher.